PAN
ARCHIVES OF ACOUSTICS
Vol. **45**, No. 1, pp. 35–48 (2020)
DOI: 10.24425/aoa.2020.132480

Research Paper

Repetitive Acoustic Streaming Patterns in Sinusoidal Shaped Microchannels

Elnaz Attar JANNESAR[(1)], Hossein HAMZEHPOUR[(1),(2)*]

[(1)] *Department of Physics*
K.N. Toosi University of Technology
Tehran 15875-4416, Iran

[(2)] *School of Physics*
Institute for Research in Fundamental Sciences (IPM)
Tehran 19395-5531, Iran
*Corresponding Author e-mail: hamzehpour@kntu.ac.ir

(*received October 12, 2019; accepted December 4, 2019*)

Geometry of the fluid container plays a key role in the shape of acoustic streaming patterns. Inadvertent vortices can be troublesome in some cases, but if treated properly, the problem turns into a very useful parameter in acoustic tweezing or micromixing applications. In this paper, the effects of sinusoidal boundaries of a microchannel on acoustic streaming patterns are studied. The results show that while top and bottom sinusoidal walls are vertically actuated at the resonance frequency of basic hypothetical rectangular microchannel, some repetitive acoustic streaming patterns are recognised in classifiable cases. Such patterns can never be produced in the rectangular geometry with flat boundaries. Relations between geometrical parameters and emerging acoustic streaming patterns lead us to propose formulas in order to predict more cases. Such results and formulations were not trivial at a glance.

Keywords: acoustic streaming; sinusoidal boundaries; microscale vortices; sub-microparticle trapping.
PACS number: 43.25.+y, 43.25.Nm, 43.20.Fn, 47.15.-x.

1. Introduction

Ultrasound acoustic standing waves are used to generate two nonlinear acoustophoretic forces for manipulation of fluids and particles inside microfluidic systems (Czyż, 1987a; 1987b; Lewandowski, 1992; Wiklund *et al.*, 2012; Włoch *et al.*, 2019). The acoustic radiation force tends to focus particles on the nodal or anti-nodal plane of the acoustic standing waves (Doinikov, 1997; Gor'kov, 1962; King, 1934; Yosioka, Kawasima, 1955) while the Stokes drag force of the acoustic streaming velocity field tends to defocus and spread out the suspended particles (Nyborg, 1953; 1958; Rayleigh, 1884; Schlichting, Gersten, 2017). Critical particle diameter is determined as a crossover from the radiation force dominated region to the acoustic streaming-induced drag force dominated region (Barnkob *et al.*, 2012; Spengler *et al.*, 2003). Particles with diameters larger than the critical diameter are enforced with the radiation force, as this is caused by the scattering of acoustic waves from the surface of particles. On the other hand, tiny particles smaller than the critical size are affected by the acoustic streaming steady fluid flows caused by viscous stresses in acoustic boundary layers.

The classical theory of Rayleigh streaming was established for shallow infinite parallel-plate channels (Rayleigh, 1884). Schlichting streaming is modelled mathematically for single planar infinite rigid walls (Schlichting, Gersten, 2017). Many further studies have followed the same geometries (Hamilton *et al.*, 2003; Nyborg, 1958; Rednikov, Sadhal, 2011; Westervelt, 1953). Muller *et al.* (2013) have proposed a theoretical analysis of acoustic streaming with taking the effect of the vertical sidewalls into account. They published a complete description of microparticle acoustophoresis combined with wall effects.

For geometries more irregular than rectangular microchannels, the analytical studies are impossible and numerical simulations need to be employed. To date, there has been a large quantity of literature published on this topic including analytical, numerical, and ex-

perimental studies. Any changes in the boundary conditions, such as the geometry of the fluid container, dramatically affect the shape of the acoustic streaming patterns. Inadvertent vortices can be troublesome in some cases, but if treated properly, the problem turns into a very useful parameter in patterning or mixing applications (Evander, Nilsson, 2012; Wiklund *et al.*, 2012). A microchannel with the sharp edged sidewalls has been used as a micromixer (Nama *et al.*, 2014). Same geometry proposes precise rotational manipulation of cells and other micrometer sized biological samples (Feng *et al.*, 2018). Also, additional study shows that mixing performance varies at different frequencies and tip angles (Huang *et al.*, 2013). Oscillations of tilted sharp edge structures have suggested a programmable acoustofluidic pump (Huang *et al.*, 2014). Function of oscillating microbubbles have considered in some other literatures. Acoustically driven sidewall trapped microbubbles act as a fast microfluidic mixer (Ahmed *et al.*, 2009). Microbubbles inside a horseshoe structure produce acoustic streaming vortices which are able to trap bacterial aggregations (Yazdi, Ardekani, 2012). On the other hand, focusing the sub-micrometer particles and bacteria both horizontally and vertically in the cross section of a microchannel is feasible using two dimensional acoustic streaming phenomena. The single roll streaming flow is observed experimentally in a nearly square channel, and acoustophoretic focusing of E. Coli bacteria and 0.6 m particles is achieved (Antfolk *et al.*, 2014). An ultrasonic device for micro-patterning and precision manipulation of micrometer scale particles has been introduced using eight piezoelectric transducers shaped into an octagonal cavity (Bernassau *et al.*, 2013). The effects of profiled surfaces on the boundary driven streaming fields in 2D rectangular chambers have been numerically investigated by Lei *et al.* (2018). Their models predict that profiles with amplitudes comparable to the viscous boundary layer have the potential to dramatically enhance (and change the pattern of) acoustic streaming patterns.

In this work, we numerically investigate the effects of different geometrical parameters on two dimensional acoustic streaming patterns inside microchannels with acoustically oscillating sinusoidal walls in vertical direction. Some special acoustic streaming patterns emerge in the form of repetitive shapes in special cases that can never be produced in rectangular geometry with flat boundaries using one dimensional oscillations. We propose a relation between such patterns and geometrical parameters that lead us to predict much more cases. Such results for sinusoidal geometry were not trivial at a glance.

The paper is organized as follows. In Sec. 2 we derive the governing equations that are solved numerically. This is followed in Sec. 3 by description of the numerical model and considering boundary conditions. In Sec. 4 effects of three geometrical parameters are discussed that are the ratio of the side walls, symmetry or asymmetry of sinusoidal walls and geometrical wavelength of them. A formulation is suggested to make other cases predictable. Finally, an application is introduced numerically to trap sub-micron particles inside a sinusoidal microchannel in single tweezing points. Such trapping was never achieved in two dimensional cases with only one directionally oscillation of boundaries. All conclusions stated in this paper can be leading points to optimise the performance of acoustofluidic devices.

2. Theory

In the absence of external body forces and heat sources, there are three important governing equations in microfluidic systems as (Muller, Bruus, 2014)

$$\begin{aligned} \partial_t \rho &= \nabla \cdot [-\rho \mathbf{v}], \\ \partial_t (\rho \mathbf{v}) &= \nabla \cdot [\boldsymbol{\sigma} - \rho \mathbf{v}\mathbf{v}], \\ \partial_t \left(\rho\varepsilon + \frac{1}{2}\rho v^2\right) &= \nabla \cdot \left[k^{th}\nabla T + \mathbf{v}\cdot\boldsymbol{\sigma} - \rho\left(\varepsilon + \frac{1}{2}v^2\right)\mathbf{v}\right]. \end{aligned} \tag{1}$$

The continuity Eq. $(1)_1$ expresses conservation of mass where the mass current density is ρ, the Navier-Stokes Eq. $(1)_2$ expresses conservation of momentum where momentum current density is $\rho\mathbf{v}$, and the Eq. $(1)_3$ expresses conservation of energy where energy current density is $\rho\left(\varepsilon + \frac{1}{2}v^2\right)$ (Landau, Lifsitz, 1967; Muller, Bruus, 2014). ϵ is internal energy per unit mass, $\mathbf{v}$ is velocity of the fluid in the medium, and k^{th} is the thermal conductivity. Also, $\boldsymbol{\sigma}$ is the stress tensor of the fluid (Cauchy stress tensor) as

$$\boldsymbol{\sigma} = \boldsymbol{\tau} - p\mathbf{I} = \eta[\nabla\mathbf{v} + (\nabla\mathbf{v}^{\mathrm{T}}] + \left[\left(\eta^B - \frac{2}{3}\eta\right)\nabla\cdot\mathbf{v} - p\right]\mathbf{I}, \tag{2}$$

where the viscous stress tensor, $\boldsymbol{\tau}$, is expressed in terms of dynamic shear viscosity η and bulk viscosity η^B. Additionally, p is the pressure field and $\mathbf{I}$ is the unit tensor.

Thermal effects will be neglected, because the thermal boundary layer thickness (thermal diffusion length), δ_t, in fluids is much smaller than viscous boundary layer thickness (viscous penetration depth), δ_ν that are defined as (Muller *et al.*, 2012)

$$\begin{aligned} \delta_t &= \sqrt{\frac{2D_{th}}{\omega}}, \\ \delta_\nu &= \sqrt{\frac{2\nu}{\omega}}, \end{aligned} \tag{3}$$

where D_{th} is the thermal diffusion constant, ω is angular frequency of the acoustic field and $\nu = \frac{\eta}{\rho}$ is the dynamic viscosity.

Considering the external acoustic field as a perturbation of the steady state of a fluid, all the fields can be expanded as $g = g_0 + g_1 + g_2$ taking the first and second order (subscript 1 and 2, respectively) into account. We expand the non-linear fluid equations to the second order.

For a medium with the speed of sound c_0, the magnitude of the perturbation can be characterised by the dimensionless acoustic Mach number (Landau, Lifshitz, 1967) as

$$\mathrm{Ma} = \frac{v_1}{c_0} = \frac{|\rho_1|}{\rho_0} \ll 1, \tag{4}$$

where ρ_0 is the unperturbed density of the fluid and ρ_1 is the first order perturbation term of density. Ignoring thermal effects, the first order perturbation approximations of governing equations in frequency domain are (Muller, Bruus, 2015)

$$\begin{aligned} \nabla \cdot \mathbf{v}_1 - i\omega\kappa_0 p_1 &= 0, \\ \nabla \cdot \boldsymbol{\sigma}_1 + i\omega\rho_0 \mathbf{v}_1 &= 0. \end{aligned} \tag{5}$$

The acoustic pressure is calculated as $p_1 = c_0^2\rho_1$ and $\kappa_0 = \frac{1}{\rho}\left(\frac{\partial\rho}{\partial p}\right)_s = \frac{1}{\rho_0 c_0^2}$ is isentropic compressibility where c_0 is the speed of sound in water at rest. Using the first order approximation of the perturbation theory, the stress tensor is calculated as

$$\begin{aligned} \boldsymbol{\sigma}_1 &= \boldsymbol{\tau}_1 - p_1\mathbf{I} = \eta_0\left[\nabla\mathbf{v}_1 + (\nabla\mathbf{v}_1)^{\mathrm{T}}\right] \\ &\quad + \left[\left(\eta_0^B - \frac{2}{3}\eta_0\right)\nabla\cdot\mathbf{v}_1 - p_1\right]\mathbf{I}, \end{aligned} \tag{6}$$

where zero indices refer to the properties at the equilibrium. The time averaged second order perturbation approximations of governing equations in frequency domain are (Muller, Bruus, 2015)

$$\begin{aligned} \nabla\cdot\langle\mathbf{v}_2\rangle + \kappa_0\langle\mathbf{v}_1\cdot\nabla p_1\rangle &= 0, \\ \nabla\cdot\left[\boldsymbol{\sigma}_2 - \rho_0\langle\mathbf{v}_1\mathbf{v}_1\rangle\right] &= 0. \end{aligned} \tag{7}$$

The stress tensor of the fluid using the second order perturbation theory is defined as

$$\begin{aligned} \boldsymbol{\sigma}_2 &= \boldsymbol{\tau}_2 - p_2\mathbf{I} = \eta_0\left[\nabla\mathbf{v}_2 + (\nabla\mathbf{v}_2)^{\mathrm{T}}\right] \\ &\quad + \left[\left(\eta_0^B - \frac{2}{3}\eta_0\right)(\nabla\cdot\mathbf{v}_2) - p_2\right]\mathbf{I}, \end{aligned} \tag{8}$$

where η_1^B and η_1 are the bulk viscosity and dynamic shear viscosity of the fluid, respectively. As mentioned above, in adiabatic thermodynamic approximation, the thermal term is ignored. Resulting expression for the acoustic radiation force on a spherical particle with radius of a is obtained by (Muller *et al.*, 2012; Settnes, Bruus, 2012)

$$\begin{aligned} \mathbf{F}_{\mathrm{rad}} &= -\pi a^3\left[\frac{2\kappa_0}{3}\mathrm{Re}\left[f_1^* p_1^{*in}\nabla p_1^{in}\right]\right. \\ &\quad \left. - \rho_0\mathrm{Re}\left[f_2^*\mathbf{v}_1^{*in}\cdot\nabla\mathbf{v}_1^{in}\right]\right], \end{aligned} \tag{9}$$

where $\mathbf{v}_1^{in}$ and p_1^{in} are the first order pressure and velocity fields of the incident acoustic wave evaluated at a particle position. Asterisks denote complex conjugations. The prefactors f_1 and f_2 are the so called mono- and dipole scattering coefficients, respectively, that in viscous fluid are calculated as (Muller *et al.*, 2012; Settnes, Bruus, 2012)

$$\begin{aligned} f_1(\widetilde{\kappa}) &= 1 - \widetilde{\kappa}, && \text{with } \widetilde{\kappa} = \frac{\kappa_p}{\kappa_0}, \\ f_2(\widetilde{\rho},\widetilde{\delta_\nu}) &= \frac{2\left[1 - \Gamma(\widetilde{\delta_\nu})\right](\widetilde{\rho}-1)}{2\widetilde{\rho} + 1 - 3\Gamma(\widetilde{\delta_\nu})}, && \text{with } \widetilde{\rho} = \frac{\rho_p}{\rho_0}, \\ \Gamma(\widetilde{\delta_\nu}) &= -\frac{3}{2}\left[1 + \mathrm{i}\left(1 + \widetilde{\delta_\nu}\right)\right]\widetilde{\delta_\nu}, && \text{with } \widetilde{\delta_\nu} = \frac{\delta_\nu}{a}, \end{aligned} \tag{10}$$

where κ_p and ρ_p are the compressibility and density of the particles, respectively.

The time averaged streaming induced drag force on a spherical particle of radius a moving with velocity $\mathbf{u}$, far from the channel walls in a fluid with time averaged streaming velocity $\langle\mathbf{v}_2\rangle$ is given by (Settnes, Bruus, 2012)

$$\mathbf{F}_{\mathrm{drag}} = 6\pi\eta a(\langle\mathbf{v}_2\rangle - \mathbf{u}). \tag{11}$$

The nonlinear acoustophoretic forces compete with each other. The crossover from the dominance of each force is defined through a critical particle radius. For a fixed spherical particle inside a rectangular microchannel, the crossover diameter is (Muller *et al.*, 2012)

$$2a_c = \sqrt{12\frac{\Psi}{\Phi}}\delta_\nu, \tag{12}$$

where Ψ is a factor related to the channel geometry. The acoustophoretic contrast factor is calculated as $\Phi(\widetilde{\kappa},\widetilde{\rho},\widetilde{\delta_\nu}) = \frac{1}{3}f_1(\widetilde{\kappa}) + \frac{1}{2}f_2^r(\widetilde{\rho},\widetilde{\delta_\nu})$ that contains material parameters. The monopole scattering coefficient, f_1, is real valued and depends only on the compressibility ratio between the particle and the fluid, $\widetilde{\kappa}$ but the viscosity dependent dipole scattering coefficient, f_2, is in general a complex valued number, and its real value is abbreviated as $f_2^r(\widetilde{\rho},\widetilde{\delta_\nu}) = \mathrm{Re}\left[f_2(\widetilde{\rho},\widetilde{\delta_\nu})\right]$.

3. Numerical model and boundary conditions

In the following, a numerical model is presented for microchannels with actuating sinusoidal top and bottom walls. Finite element method is one of the most widely used numerical methods in computational simulations. In this study, the same method is utilised

considering the weak form of the partial differential equations.

Two examples of sinusoidal microchannels are sketched in Fig. 1. Top and bottom walls have symmetrical or asymmetrical sinusoidal forms given by the functions

$$z = \pm\left(\frac{h}{2}\right) \pm A\sin\left(\frac{2m\pi y}{w} + \phi_g\right), \quad m = \frac{1}{4}, \frac{1}{2}, \frac{3}{4}, 1, ..., \tag{13}$$

where A is the amplitude of the sinusoidal boundaries, w is the width of the microchannels, h is the height of corresponding hypothetical rectangular microchannels, which is considered 100 μm in this study, and ϕ_g is a geometrical phase parameter, typically equals to zero. Noteworthy, first ± sign in Eq. (11) refers to top or bottom boundaries, and the minus sign in second ± in the equation belongs to the bottom walls of asymmetrical microchannels.

The governing Eqs (5), (7) are solved using the finite element method. We have used the weak-form-PDE of mathematics for both first and second order equations. The conducted steps are as follows: First, the flow equations are written as source free flux formulation, $\nabla\cdot\mathbf{J} + F = 0$; then they are converted to the weak form; finally, the weak form equations are solved by mathematics weak form PDE module. In all cases, the zero flux boundary condition, $\mathbf{J}\cdot\mathbf{n} = 0$, is supposed where $\mathbf{n}$ is the normal vector to the boundary surface. Also, all boundaries are considered as hard walls.

Top and bottom walls are actuated by an external acoustic field at the frequency of f_v, which is the vertical resonance frequency of a hypothetical rectangular microchannel with a height of h. The boundary conditions of the first order velocity field are:

$$\begin{aligned} &\text{top–bottom}: \quad v_{y1} = 0, \quad v_{z1} = v_{bc}\sin(\omega t),\\ &\text{left–right}: \quad v_{y1} = 0, \quad v_{z1} = 0, \end{aligned} \tag{14}$$

where $v_{bc} = \omega d$, $\omega = 2\pi f$, and $d = 0.1$ nm. The displacement of the oscillating walls in the z direction, d, is small enough to use the perturbation theory.

A zero mass flux boundary condition is considered for the second order velocity field as

$$\begin{aligned} &\text{top-bottom}: \quad v_{y2} = 0, \quad v_{z2} = -\frac{\langle\rho_1 v_{z1}\rangle}{\rho_0},\\ &\text{left-right}: \quad v_{y2} = 0, \quad v_{z2} = 0. \end{aligned} \tag{15}$$

The maximum mesh size in boundaries until $10\delta_\nu$ and bulk are considered 0.5 μm and 5 μm, respectively. The mesh element growth rate is 1.3 (see Fig. 2).

The fluid inside the microchannel is considered to be quiescent water. Also, the physical parameters for water at the temperature of $T = 25°\text{C}$ and pressure $p_0 = 0.1013$ MPa are shown in Table 1.

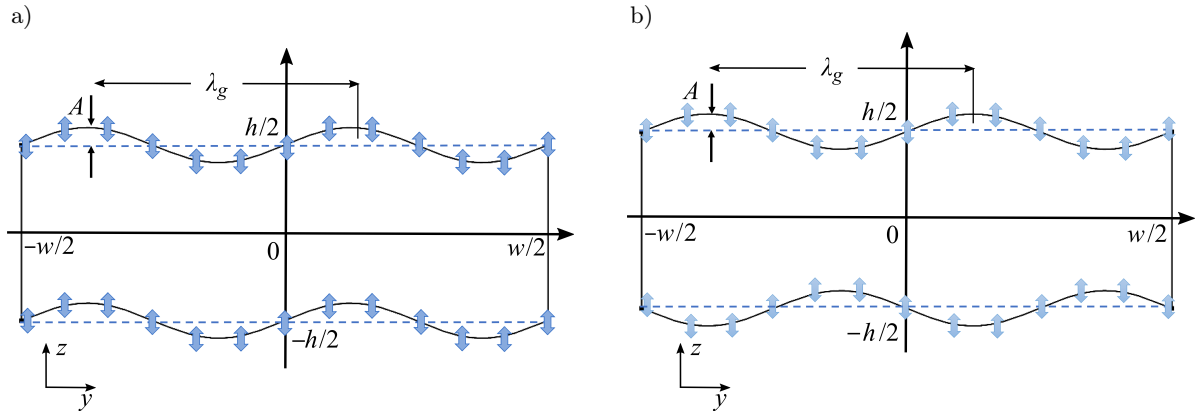

Fig. 1. Two dimensional schematics of microchannels in yz plane are shown. Top and bottom walls are (a) symmetrically and (b) asymmetrically sinusoidal. Blue arrows show the oscillation direction of the actuated boundary walls at the resonance frequency of f_v. Hypothetical basic rectangular microchannels are shown by dashed lines with the height of h and width of w. λ_g is defined as the geometrical wavelength of sinusoidal shaped boundaries.

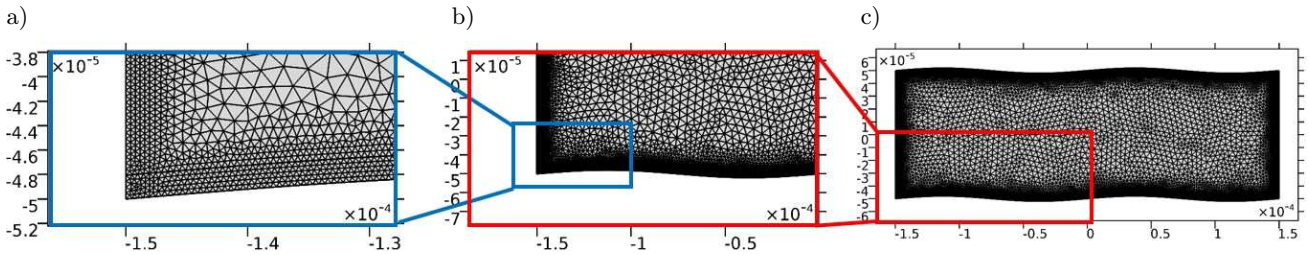

Fig. 2. (a) Sketch of the spatial mesh of the sinusoidal computational domain in the yz plain. (b) and (c) are two zoom in scales on the mesh in the lower left corner.

Table 1. Physical parameters of water at $T = 25°C$ and $p_0 = 0.1013$ MPa (Muller, Bruus, 2014).

Parameter	Symbol	Value	Unit
Mass density	ρ_0	$9.970 \cdot 10^2$	kg/m^3
Speed of sound	c_0	$1.497 \cdot 10^3$	m/s
Shear viscosity	η_0	$8.900 \cdot 10^{-4}$	Pa·s
Bulk viscosity	η_0^B	$2.485 \cdot 10^{-3}$	Pa·s

4. Results and discussion

Acoustic streaming vortices can be troublesome in some cases, but if controlled and treated properly, the problem turns into a beneficial parameter in acoustic tweezing or micromixing applications. Concerning the fact that the acoustic streaming patterns are extremely sensitive to the geometry of the fluid container, extensive numerical calculations were carried out to study such effects on acoustic streaming patterns in two dimensions. In what follows we present the results and discuss their implications.

4.1. Effective parameters on acoustic streaming patterns of sinusoidal microchannels

The parameters which can affect streaming patterns in a microchannel with sinusoidal boundaries are the applied frequency, f, microchannel's width to height ratio, $n = w/h$, amplitude of the sinusoidal walls, A, symmetry or asymmetry of the sinusoidal walls, and geometrical wavelength, λ_g. In this study, f_v and A are considered constant equal to $c/2h$ and $h/50$ respectively, where c is the speed of sound in water. Effects of other parameters are investigated in details as follows.

4.1.1. Effects of the microchannel's width to height ratio, n

Figures 3 and 4 illustrate examples for two fixed geometrical wavelengths, $\lambda_g = 2w$ and $\lambda_g = w$, but different values of n from 1 to 5 for each case. The results show that in some various microchannel's width to height ratios the streaming patterns are completely different from the flat geometry streaming patterns. Dominant repetitive vortices or twisting-like patterns are discoverable. For $\lambda_g = 2w$ and odd numbers of n, streaming patterns tend to flat geometry. For $\lambda_g = w$ and even numbers of n the same results are achieved.

Acoustic streaming patterns for other geometrical wavelengths with variable ratios have been studied numerically and the same pattern sequences have been extracted. The details will be discussed further to classify and formulate such appearing streaming patterns.

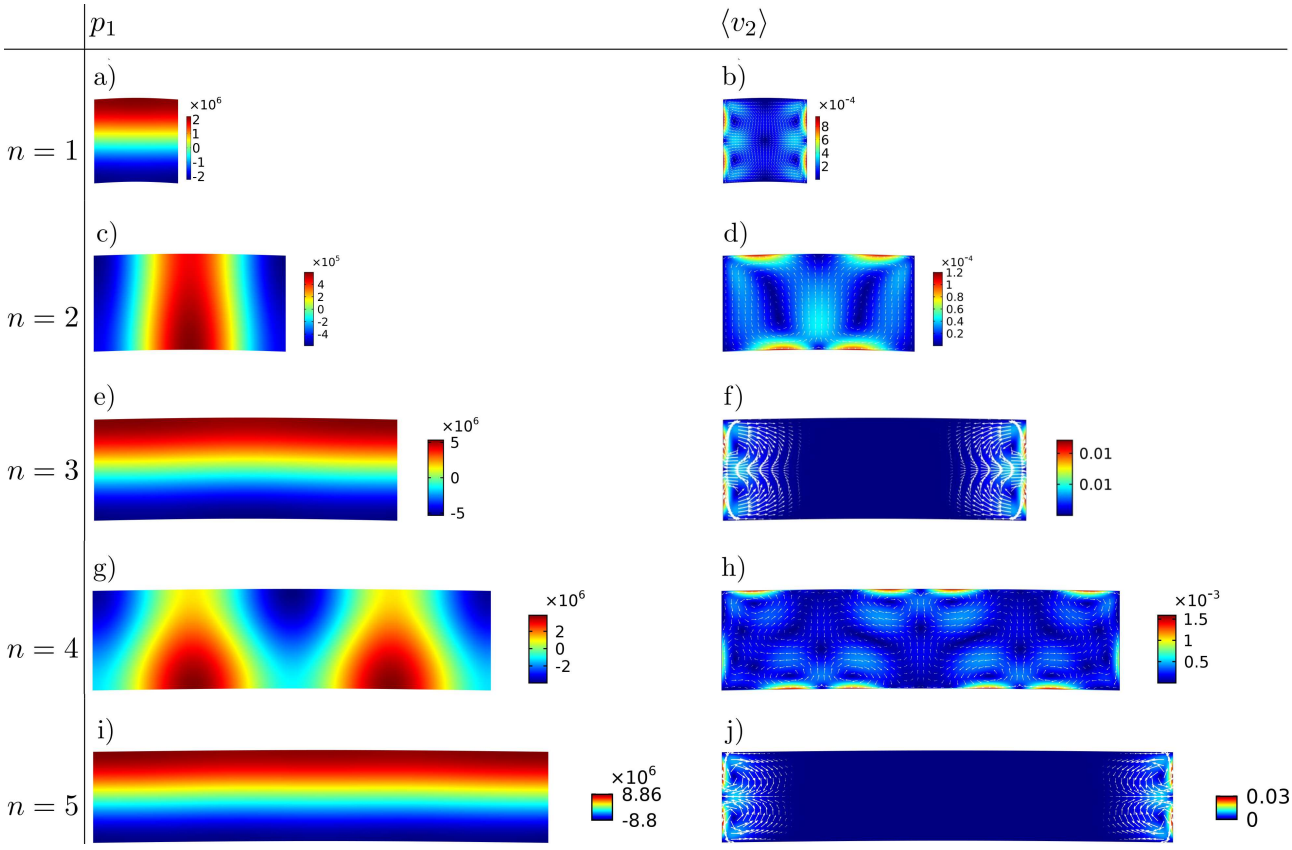

Fig. 3. First order pressure fields (left column) and time averaged second order velocity fields (right column) in cross section of sinusoidal microchannels where geometrical wavelengths of symmetrical top and bottom walls remain fixed as $\lambda_g = 2w$ and the microchannel's width to height ratio, n, varies from 1 to 5.

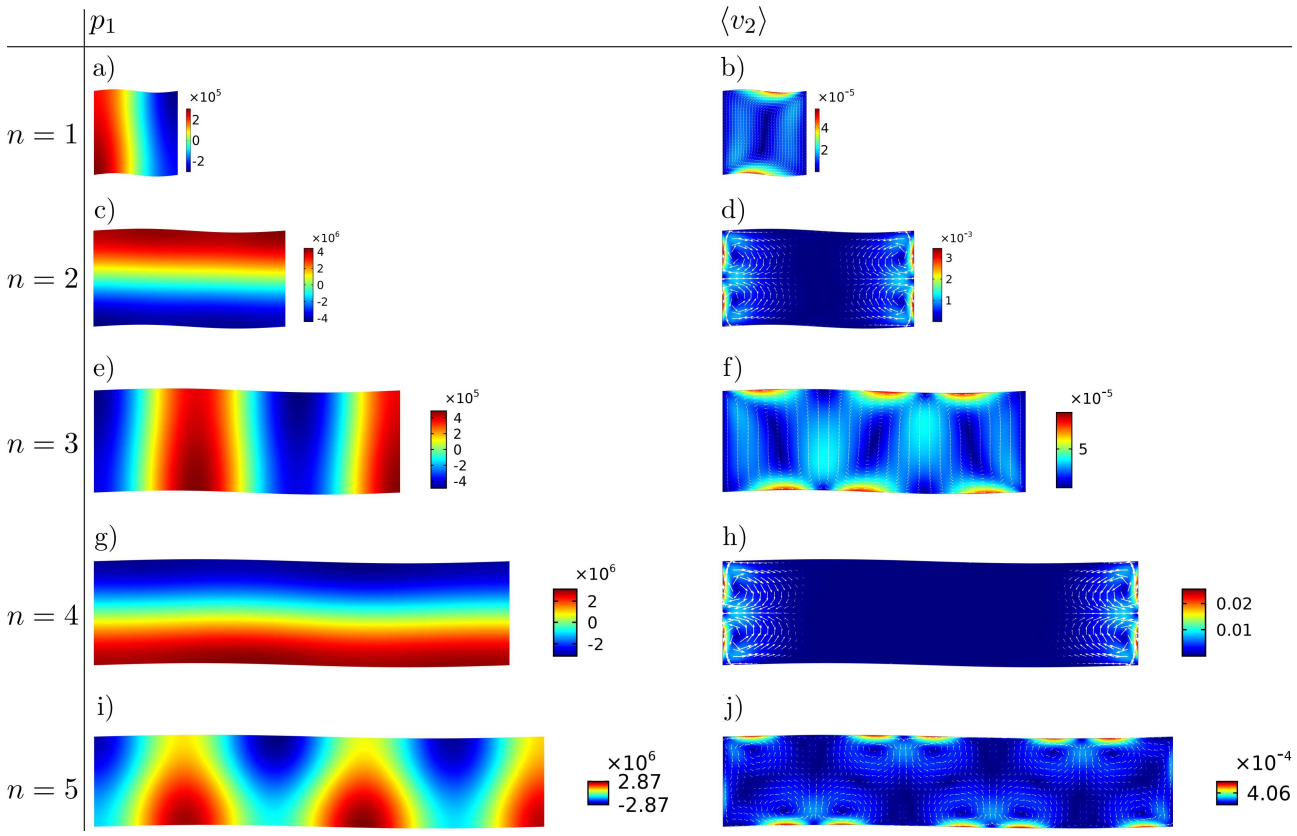

Fig. 4. First order pressure fields (left column) and time averaged second order velocity fields (right column) in cross section of sinusoidal microchannels where geometrical wavelengths of symmetrical top and bottom walls remain fixed as $\lambda_g = w$ and the microchannel's width to height ratio, n, varies from 1 to 5.

4.1.2. Effects of geometrical wavelength on acoustic streaming patterns

Another investigation was carried out with focusing on the different values of λ_g but fixed n. The results show that λ_g definitely affects streaming patterns in some cases. Dominant repetitive vortices and twisting-like patterns are discoverable similar to the cases with fixed λ_g but changing n. In some repetitive cases patterns resemble flat geometry pattern. Figure 5 shows the results for $n = 6$ and definitive magnitudes of λ_g. As depicted, acoustic standing waves rotate in some cases from vertical into horizontal. Noteworthy, the frequency of actuation and the direction of oscillations are vertical in all cases. Further investigation shows that the patterns in $n = 6$ are achievable in other channel widths with classifiable values of λ_g. As a result, some formulations are proposed in Subsec. 4.2 to make acoustic streaming patterns predictable as much as possible.

4.1.3. Effects of asymmetrical sinusoidal top and bottom walls

The same simulations as above were repeated for asymmetrical sinusoidal boundaries. Figure 6 indicates cases with different values of n but fixed λ_g and Fig. 7 shows selected simulations for different values of λ_g but fixed n. The results declare that in asymmetrical cases previous patterns, as in symmetrical boundaries, are not achievable. The generating standing waves typically resemble flat geometry and streaming patterns carry less deviation from a rectangular case as compared to the symmetrical cases. However, some considerable patterns exist. At the geometrical wavelength of $\lambda_g = 2w$ but high numbers of n four additional boundary layers generate around the sinusoidal curved boundaries. As a result, four bulk streaming flows emerge in the bulk of the microchannel. In addition, at $\lambda_g = w$, some stretched fluid circles are generated as in Fig. 7d. As such, fluid molecules or tiny particles transfer from one side to another side just through implying acoustical oscillations.

4.2. Classification of streaming patterns in symmetrical sinusoidal microchannels

This work aims to characterise the effect of sinusoidal boundaries on the acoustic streaming patterns in microfluidic systems. Focusing on natural values of the microchannel's width to height ratio from 1 to 10, and geometrical length-widths of $\lambda_g = 4w/2p$, where

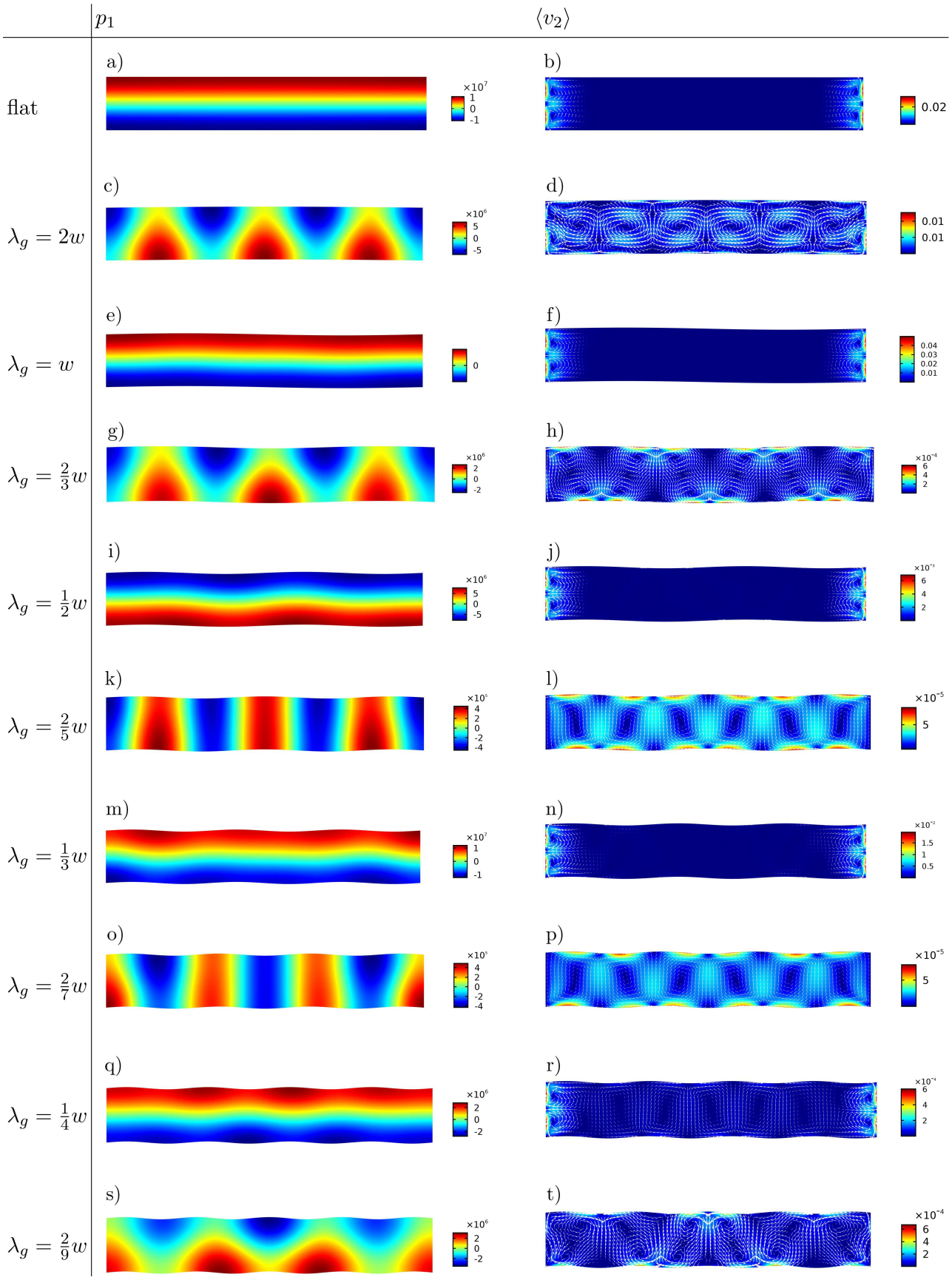

Fig. 5. First order pressure fields (left column) and time averaged second order velocity fields (right column) in cross section of sinusoidal microchannels where the microchannel's width to height ratio remains fixed as $n = 6$ and geometrical wavelengths of symmetrical top and bottom walls are $\lambda_g = 4w/2p$ where $p = 1, 2, ..., 7$.

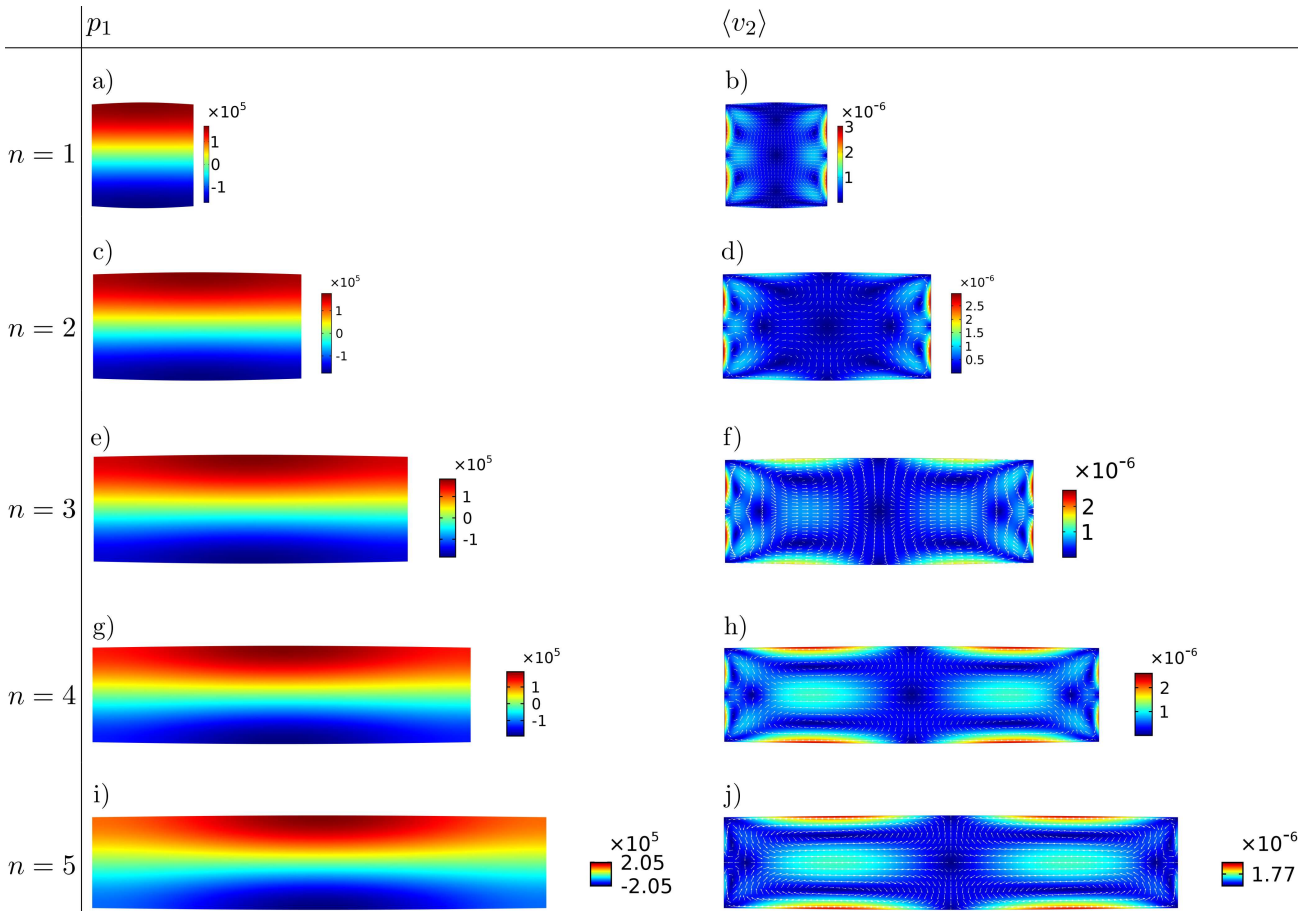

Fig. 6. First order pressure fields (left column) and time averaged second order velocity fields (right column) in cross section of sinusoidal microchannels where geometrical wavelengths of asymmetrical top and bottom walls remain fixed as $\lambda_g = 2w$ and the microchannel's width to height ratio, n, varies from 1 to 5.

$p = 1, 2, ..., 10$, leads to a 10×10 matrix which contains numerical results. A classification is proposed to predict patterns with larger values of λ_g and n through an inductive reasoning.

The first formula is declared for fast streaming patterns like Fig. 5d. It resembles a chain with n numbers of rings

$$\lambda_g = \frac{4}{2n-10} w, \tag{16}$$

where $n \geq 6 \in R$.

The next formula is proposed for the patterns like Fig. 5l where n numbers of dominant vortices are recognizable

$$\lambda_g = \frac{4}{2n-2} w, \tag{17}$$

where $n \geq 2 \in R$.

Similar patterns, with a one vortex forward shift, exist, as shown in Fig. 5p. The formulation is

$$\lambda_g = \frac{4}{2n+2} w, \tag{18}$$

where $n \geq 1 \in R$.

Another series of similar patterns could be defined considering that two corresponding vortices are generated instead of one dominant vortex as in two previous classes

$$\lambda_g = \frac{4}{2n-6} w, \tag{19}$$

where $n \geq 4 \in R$.

The next formula is defined for identical patterns imposing a shift of one vortex forward, ssee Fig. 5t

$$\lambda_g = \frac{4}{2n+6} w, \tag{20}$$

where $n \geq 1 \in R$.

For the cases very similar to flat geometry, a general relation can be proposed as

$$\lambda_g = \frac{4}{2p-1} w, \tag{21}_1$$

where $p \geq 1 \in R$ for odd numbers of n;

$$\lambda_g = \frac{4}{2p} w, \tag{21}_2$$

where $p \geq 1 \in R$ for even numbers of n.

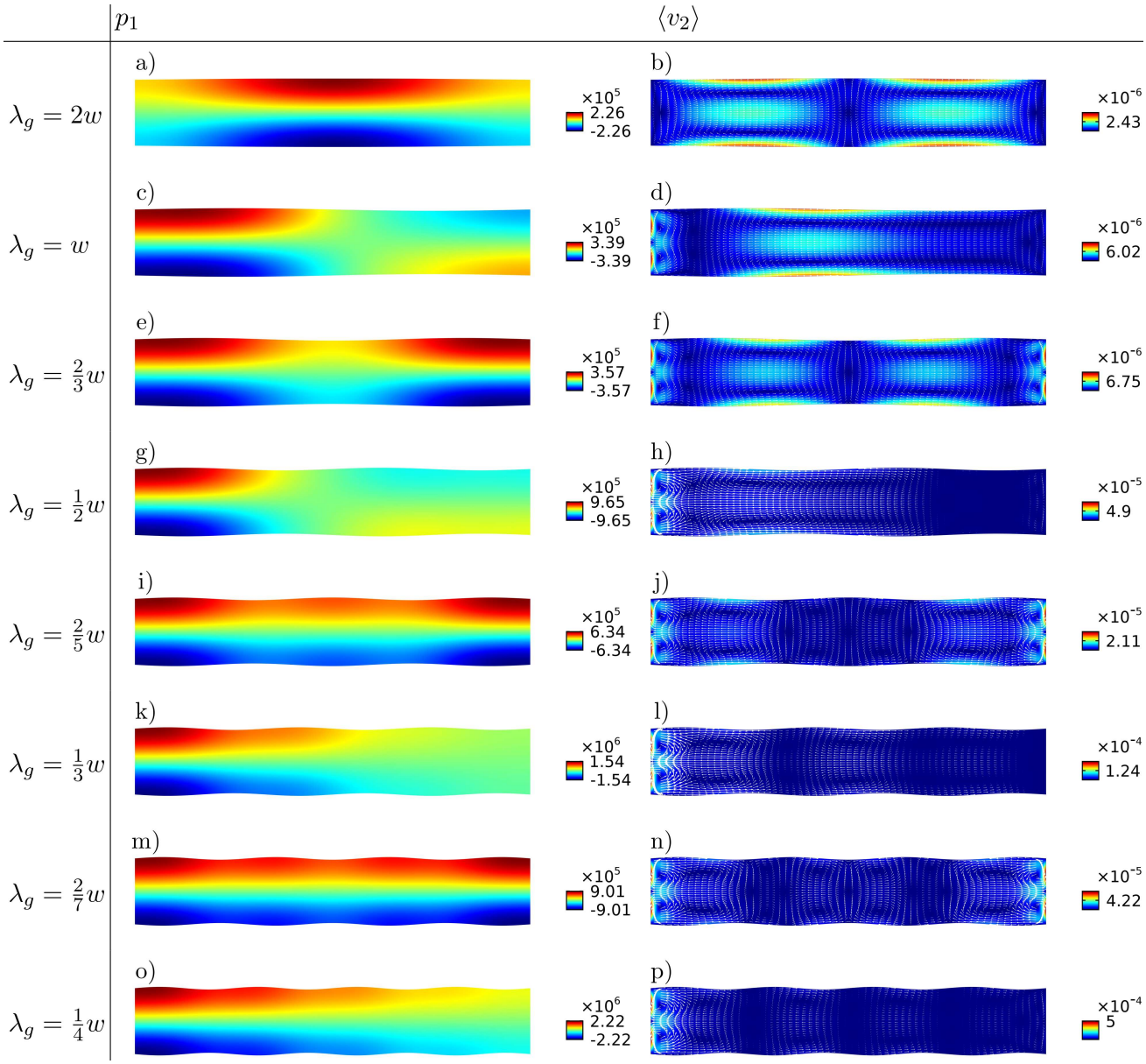

Fig. 7. First order pressure fields (left column) and time averaged second order velocity fields (right column) in cross section of sinusoidal microchannels where the microchannel's width to height ratio remains fixed as $n = 6$ and geometrical wavelengths of assymetrical top and bottom walls are $\lambda_g = 4w/2p$, where $p = 1, 2, ..., 8$.

Figure 8 validates Eq. (15) of acoustic streaming classified patterns. A single vortex is accessible when $n = 1$ and $\lambda_g = 4w$ in addition to the proposed formula.

Noteworthy, other cases with half numbers of n or geometrical wavelengths of $\lambda_g = 4w/(2p-1)$ with $p = 1, 2, ..., 10$, could be investigated. The same classification could be defined but be ignored in this study.

4.3. Investigation of microchannel's building blocks

It might be supposed that repetitive patterns could be generated when some building blocks with a single vortex pattern are joined to make a long sinusoidal microchannel. In this section, it is clarified that the repetition of acoustic streaming patterns happens in a non trivial manner. See Fig. 9 where a microchannel with $n = 4$ and $\lambda_g = w$ is separated into four microchannels with $n = 1$ and $\lambda_g = 4w$.

Figure 10 shows the results when two blocks are joined. The patterns are satisfying in this case and two dominant vortices function normally with the same order of magnitude. As the third block is added, each dominant vortex separates into two vortices. Adding the fourth block destructs all the patterns and the resulting pattern becomes the same as in the rectangular

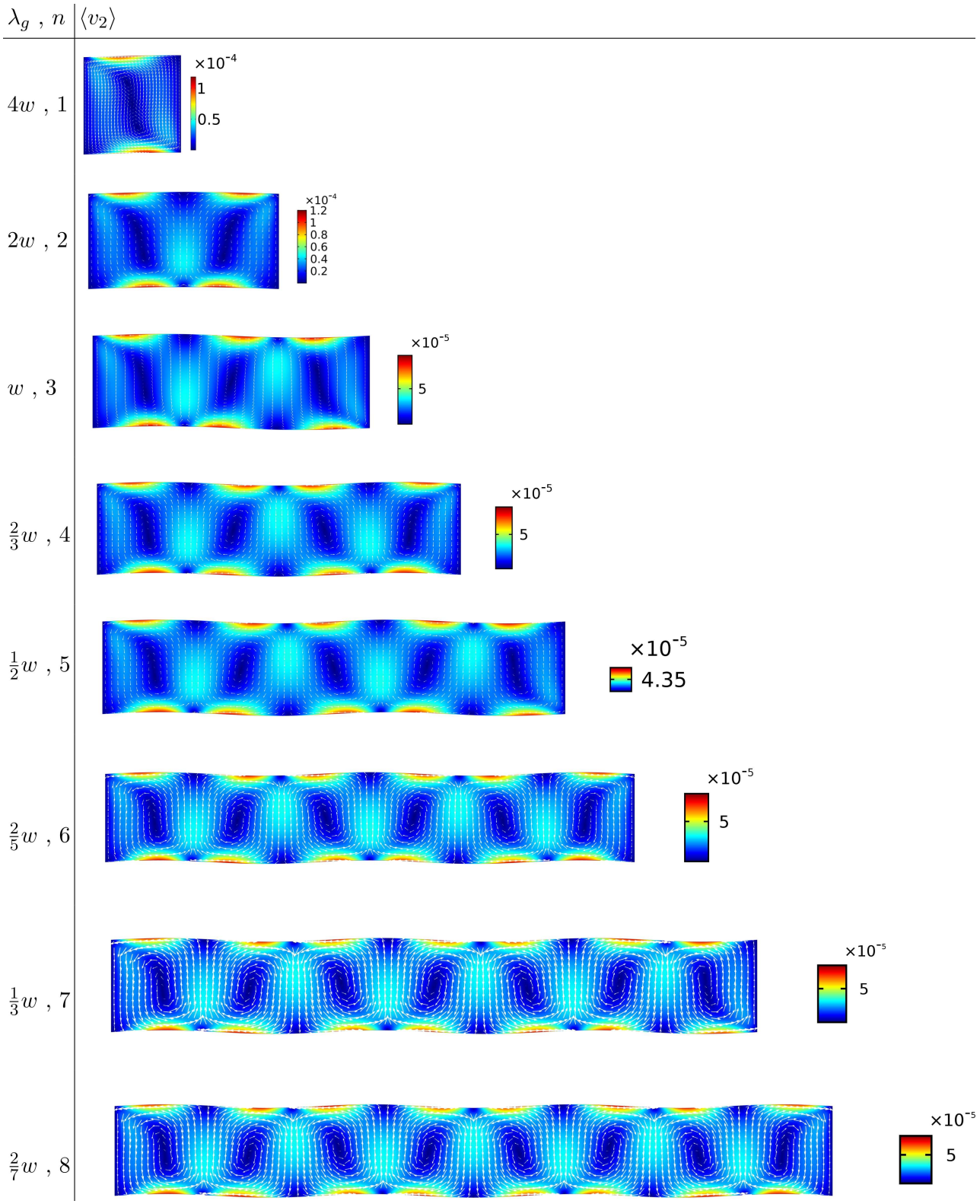

Fig. 8. Example of repetitive acoustic streaming patterns inside sinusoidal microchannels when the relation between geometrical wavelengths λ_g and the microchannel's width to height ratio is defined as $\lambda_g = 4w/(2n-2)$, where $n \geq 2 \in R$.

case. Surprisingly, adding the fifth block, makes bulk vortices emerge again, see Fig. 11.

One other example for different behaviour of joined building blocks as compared with separated ones is

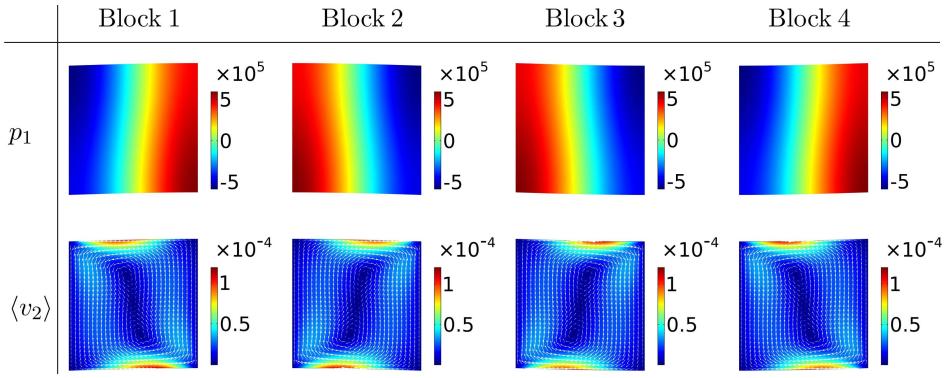

Fig. 9. First order pressure field, p_1, and acoustic streaming velocity fields, $\langle v_2 \rangle$, for building blocks of a symmetrical sinusoidal microchannel with $n = 4$ and $\lambda_g = w$. Each block has microchannel's width to height ratio of $n = 1$ and geometrical wavelength of $\lambda_g = 4w$. Geometrical phases for Block 1 to Block 4 are $\phi_g = 0, \pi/2, \pi, 3\pi/2$, respectively.

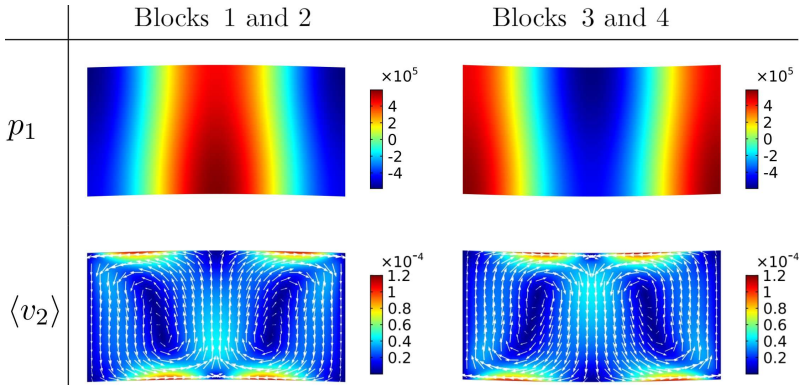

Fig. 10. First order pressure field, p_1, and acoustic streaming velocity field, $\langle v_2 \rangle$, for two adjacent building blocks of a symmetrical sinusoidal microchannel. The final blocks have microchannel's width to height ratio of $n = 2$ and geometrical wavelength of $\lambda_g = 2w$.

shown in Fig. 12, where each block has $n = 1$ and $\lambda_g = w$.

4.4. Trapping submicrometer particles inside symmetrical sinusoidal microchannels

Novel acoustic streaming repetitive patterns have been introduced numerically earlier in this paper. Patterns with repetitive single dominant vortices are capable of trapping submicron particles inside a sinusoidal microchannel in tweezing points. The most important finding is that such a trapping is now possible through modification of the geometry of the boundaries instead of adding more oscillating boundaries. Several attempts have been made to create such patterns using multiple actuators with flat geometry (Antfolk *et al.*, 2014; Bernassau *et al.*, 2013). A two dimensional cross section of a sinusoidal microchannel with 1 mm width and geometrical wavelength of $2w/9$ is shown in Fig. 13. The top and bottom sinusoidal walls are actuated at the frequency of $f_v = c/2h$.

The snapshots after 10 seconds for simulation of particles with the radius of $a = 0.25$ µm inside the microchannel indicate that submicrometer particles tend to focus being affected by acoustic streaming fluid flows, see Fig. 13d.

5. Conclusion

In this paper, we aimed at numerically characterising two dimensional acoustic streaming patterns generated in the fluid inside the microchannels with acoustically oscillating sinusoidal boundaries. Considering the fact that the acoustic streaming patterns are extremely sensitive to the geometry, some geometrical parameters have been investigated such as the microchannel's width to height ratio, symmetry or asymmetry of sinusoidal walls, and geometrical wavelength of sinusoidal boundaries. The results indicate that while the top and bottom sinusoidal boundaries had been actuated vertically at the resonance frequency of a basic hypothetical rectangular microchannel, some repetitive acoustic streaming patterns were generated. Such patterns could have never been produced in the rectangular geometry with flat boundaries with only one directional

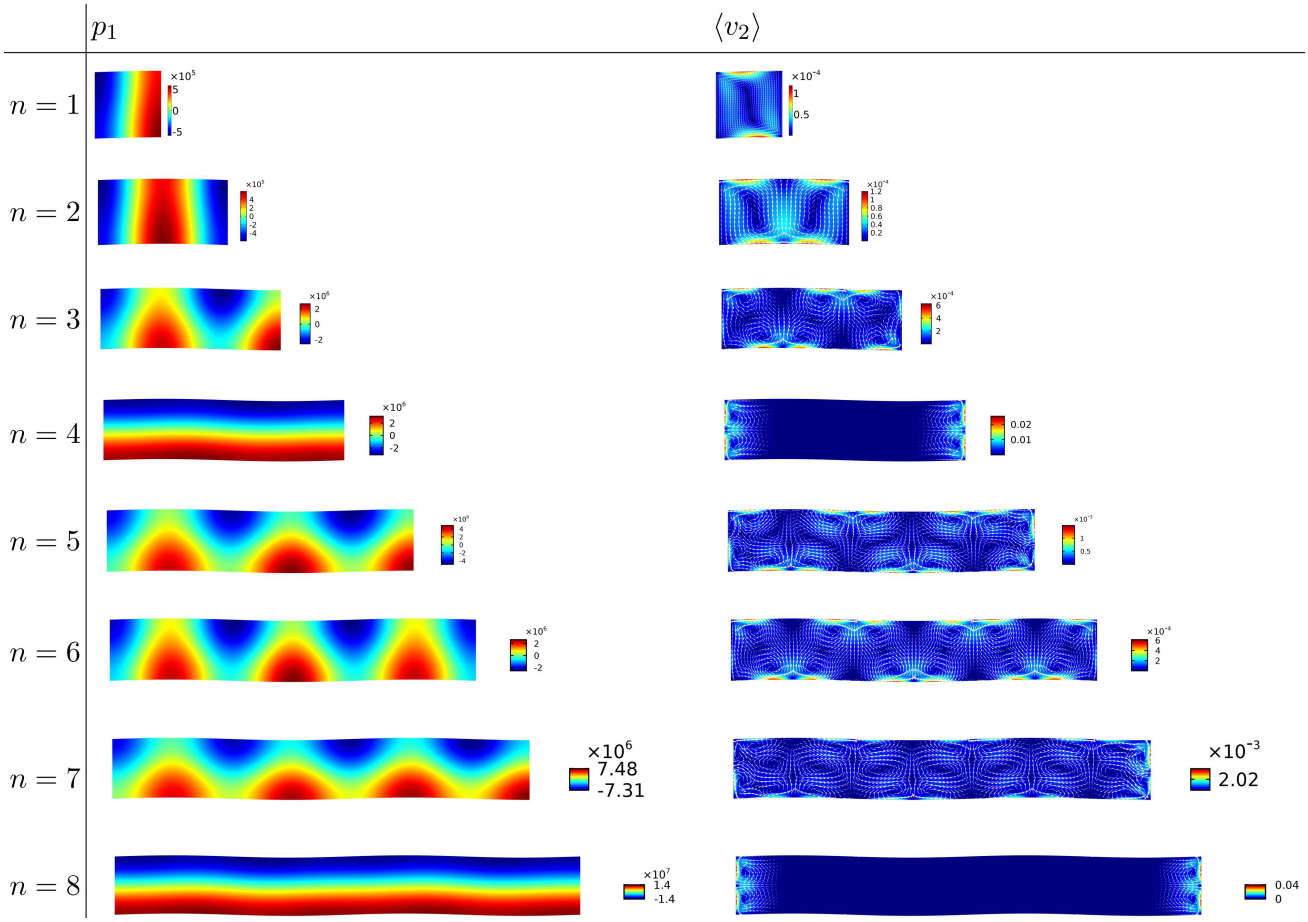

Fig. 11. Examples of p_1 and $\langle v_2 \rangle$ when adding building blocks of Fig. 9 one by one from n = 1 to n = 8. Each block has geometrical wavelength of $\lambda_g = 4w$.

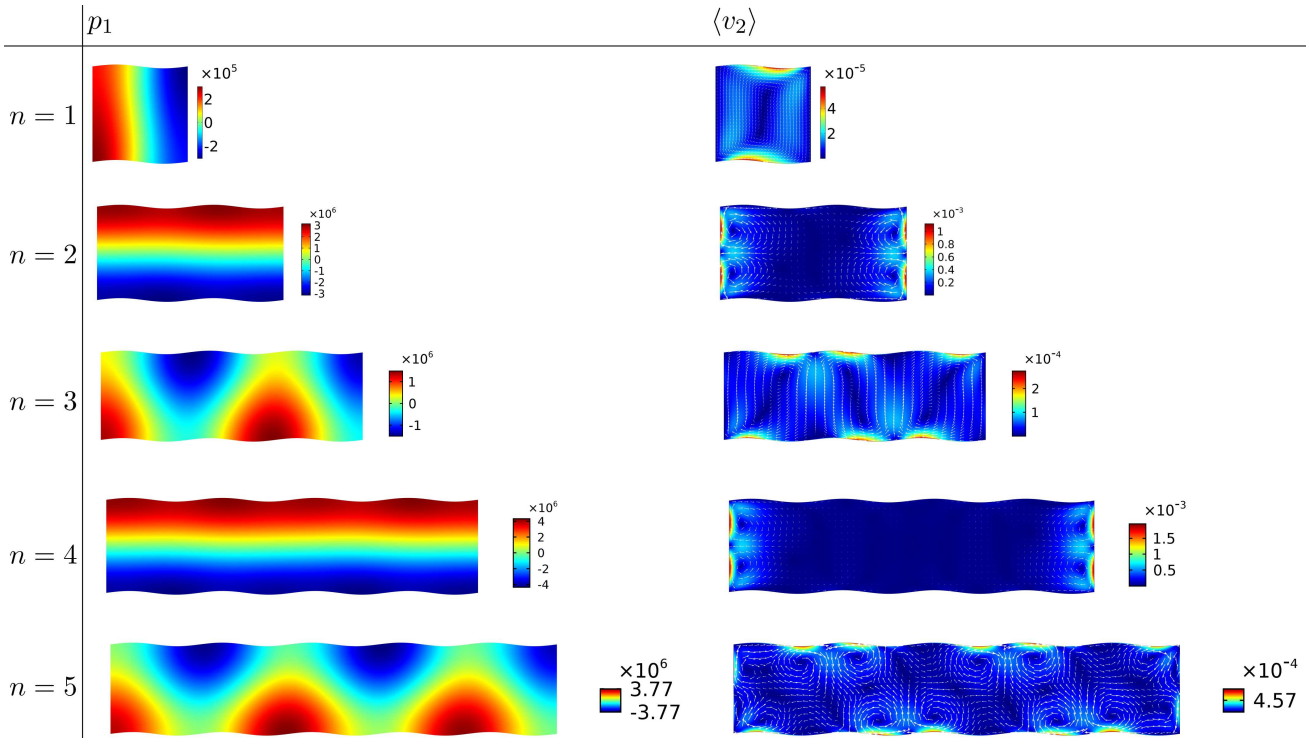

Fig. 12. Examples of p_1 and $\langle v_2 \rangle$ when adding building blocks one by one from n = 1 to n = 5. Each block has geometrical wavelength of $\lambda_g = w$.

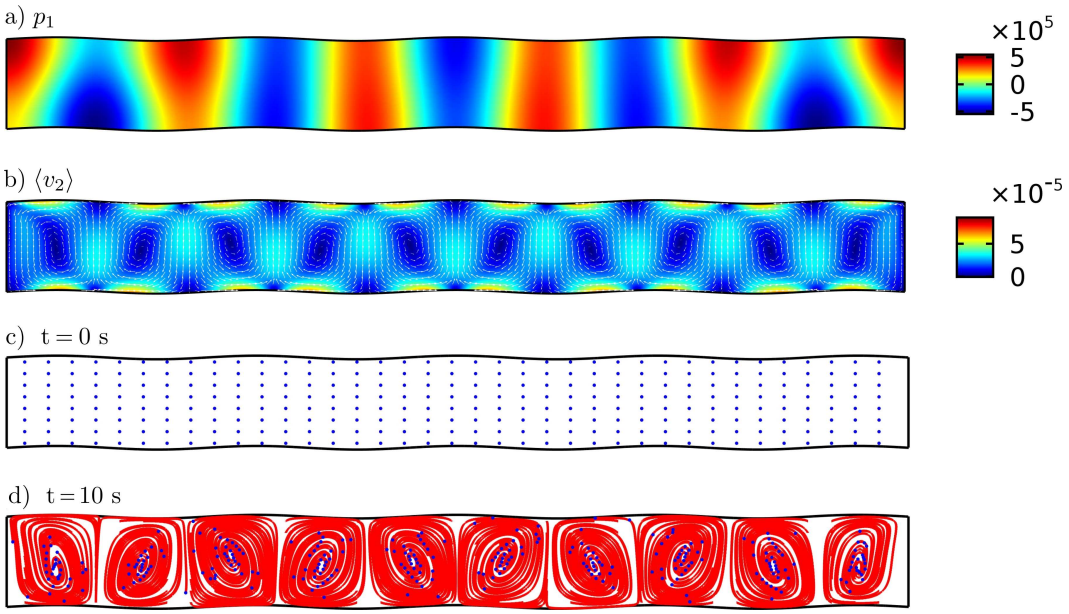

Fig. 13. a) First order pressure field, b) time-averaged second order velocity field, c) snapshot of movement of particles with the radius of a = 0.25 µm at t = 0, and d) the snapshot at t = 10 s for a symmetrical sinusoidal microchannel with the geometrical wavelength of $\lambda_g = 2w/9$ and microchannel's width to height ratio of n = 10. Trapping of tiny particles become possible by manipulation of boundary geometries in a defined manner.

oscillation of boundaries. The relations between geometrical parameters and emerging acoustic streaming patterns led us to suggest some formulas in order to predict more cases. The results and formulations were not trivial at a glance. Consequently, an application has been proposed numerically to trap sub-micron particles inside a sinusoidal microchannel in some tweezing points. All conclusions stated in this paper can be leading points to optimise the performance of acoustofluidic devices.

References

1. Ahmed D., Mao X., Juluri B.K., Huang T.J. (2009), A fast microfluidic mixer based on acoustically driven sidewall-trapped microbubbles, *Microfluidics and Nanofluidics*, **7**(5): 727, doi:10.1007/s10404-009-0444-3.
2. Antfolk M., Muller P.B., Augustsson P., Bruus H., Laurell T. (2014), Focusing of submicrometer particles and bacteria enabled by two-dimensional acoustophoresis, *Lab on a Chip*, **14**(15): 2791–2799, doi: 10.1039/C4LC00202D.
3. Barnkob R., Augustsson P., Laurell T., Bruus H. (2012), Acoustic radiation- and streaming-induced microparticle velocities determined by microparticle image velocimetry in an ultrasound symmetry plane, *Physical Review E*, **86**(5): 56307, doi: 10.1103/PhysRevE.86.056307.
4. Bernassau A.L., Courtney C.R.P., Beeley J., Drinkwater B.W., Cumming D.R.S. (2013), Interactive manipulation of microparticles in an octagonal sonotweezer, *Applied Physics Letters*, **102**(16): 164101, doi: 10.1063/1.4802754.
5. Czyż H. (1987a), Kinetics of the transport of aerosol particles under the influence of drift forces in the standing wave field, *Archives of Acoustics*, **12**(3–4):215–224.
6. Czyż H. (1987b), The aerosol particle drift in a standing wave field, *Archives of Acoustics*, **12**(3-4): 199–214.
7. Doinikov A.A. (1997), Acoustic radiation force on a spherical particle in a viscous heat-conducting fluid. I. General formula, *The Journal of the Acoustical Society of America*, **101**(2): 713–721, doi: 10.1121/1.418035.
8. Evander M., Nilsson J. (2012), Acoustofluidics 20: applications in acoustic trapping, *Lab on a Chip*, **12**(22):4667–4676, doi: 10.1039/c2lc40999b.
9. Feng L., Song B., Zhang D., Jiang Y., Arai F. (2018), On-chip tunable cell rotation using acoustically oscillating asymmetrical microstructures, *Micromachines*, **9**(11): 596, doi: 10.3390/mi9110596.
10. Gor'kov L.P. (1962), On the forces acting on a small particle in an acoustical field in an ideal fluid, In *Soviet Physics Doklady*, Vol. 6, pp. 773–775.
11. Hamilton M.F., Ilinskii Y.A., Zabolotskaya E.A. (2003), Acoustic streaming generated by standing waves in two-dimensional channels of arbitrary width, *The Journal of the Acoustical Society of America*, **113**(1): 153–160, doi: 10.1121/1.1528928.
12. Huang P.-H. *et al.* (2014), A reliable and programmable acoustofluidic pump powered by oscillating sharp-edge structures, *Lab on a Chip*, **14**(22): 4319–4323, doi: 10.1039/C4LC00806E.

13. Huang P.-H. *et al.* (2013), An acoustofluidic micromixer based on oscillating sidewall sharp-edges, *Lab on a Chip*, **13**(19): 3847–3852, doi: 10.1039/C3LC50568E.

14. King L.V. (1934), On the acoustic radiation pressure on spheres, *Proceedings of the Royal Society of London. Series A: Mathematical and Physical Sciences*, **147**(861): 212–240, doi: 10.1098/rspa.1934.0215.

15. Landau L.D., Lifshitz E.M. (1967), *Course of Theoretical Physics, Vol. 6: Fluid Mechanics*, Pergamon.

16. Lei J., Hill M., de León Albarrán C.P., Glynne-Jones P. (2018). Effects of micron scale surface profiles on acoustic streaming, *Microfluidics and Nanofluidics*, **22**(12), article number: 140, doi: 10.1007/s10404-018-2161-2.

17. Lewandowski J. (1992), Ultrasonic waves in some biological suspensions and emulsions. *Archives of Acoustics*, **17**(1): 89–102.

18. Muller P.B., Barnkob R., Jensen M.J.H., Bruus H. (2012), A numerical study of microparticle acoustophoresis driven by acoustic radiation forces and streaming-induced drag forces, *Lab on a Chip*, **12**(22): 4617–4627, doi: 10.1039/C2LC40612H.

19. Muller P.B., Bruus H. (2014), Numerical study of thermoviscous effects in ultrasound-induced acoustic streaming in microchannels, *Physical Review E*, **90**(4): 43016, doi: 10.1103/PhysRevE.90.043016.

20. Muller P.B., Bruus H. (2015), Theoretical study of time-dependent, ultrasound-induced acoustic streaming in microchannels, *Physical Review E*, **92**(6): 63018, doi: 10.1103/PhysRevE.92.063018.

21. Muller P.B. *et al.* (2013), Ultrasound-induced acoustophoretic motion of microparticles in three dimensions, *Physical Review E*, **88**(2): 23006, doi: 10.1103/PhysRevE.88.023006.

22. Nama N., Huang P.-H., Huang T.J., Costanzo F. (2014), Investigation of acoustic streaming patterns around oscillating sharp edges, *Lab on a Chip*, **14**(15): 2824–2836, doi: 10.1039/c4lc00191e.

23. Nyborg W.L. (1953), Acoustic streaming due to attenuated plane waves, *The Journal of the Acoustical Society of America*, **25**(1): 68–75, doi: 10.1121/1.1907010.

24. Nyborg W.L. (1958). Acoustic streaming near a boundary, *The Journal of the Acoustical Society of America*, **30**(4): 329–339, doi: 10.1121/1.1909587.

25. Rayleigh, *Lord* (1884), On the circulation of air observed in Kundt's tubes, and on some allied acoustical problems, *Philosophical Transactions of the Royal Society of London*, **175**: 1–21, https://www.jstor.org/stable/109434.

26. Rednikov A.Y., Sadhal S.S. (2011), Acoustic/steady streaming from a motionless boundary and related phenomena: generalized treatment of the inner streaming and examples, *Journal of Fluid Mechanics*, **667**: 426–462, doi: 10.1017/S0022112010004532.

27. Schlichting H., Gersten K. (2017), *Boundary-layer theory*, 9th. ed., Springer-Verlag, Berlin-Heidelberg, doi: 10.1007/978-3-662-52919-5.

28. Settnes M., Bruus H. (2012), Forces acting on a small particle in an acoustical field in a viscous fluid, *Physical Review E*, **85**(1): 16327, doi: 10.1103/PhysRevE.85.016327.

29. Spengler J.F., Coakley W.T., Christensen K.T. (2003), Microstreaming effects on particle concentration in an ultrasonic standing wave, *AIChE Journal*, **49**(11): 2773–2782, doi: 10.1002/aic.690491110.

30. Westervelt P.J. (1953), The theory of steady rotational flow generated by a sound field, *The Journal of the Acoustical Society of America*, **25**(1): 60–67, doi: 10.1121/1.1907009.

31. Wiklund M., Green R., Ohlin M. (2012), Acoustofluidics 14: Applications of acoustic streaming in microfluidic devices, *Lab on a Chip*, **12**(14): 2438–2451, doi: 10.1039/C2LC40203C.

32. Włoch, A., Czyż H., Jasinski T. (2019), Separation of cells from plasma by means of ultrasonics. *Archives of Acoustics*, **44**(2): 357–363, doi: 10.24425/aoa.2019.128499.

33. Yazdi S., Ardekani A.M. (2012), Bacterial aggregation and biofilm formation in a vortical flow, *Biomicrofluidics*, **6**(4): 44114, 10.1063/1.4771407.

34. Yosioka K., Kawasima Y. (1955), Acoustic radiation pressure on a compressible sphere, *Acta Acustica united with Acustica*, **5**(3): 167–173.